Materials and Design 55 (2014) 979–986

Contents lists available at ScienceDirect

Materials and Design

journal homepage: www.elsevier.com/locate/matdes

Microstructural association between mechanical behavior with bending fracture surfaces in Astaloy CrA sintered parts alloyed by Cu and C

H. Khorsand [a], M. Ghaffari [b], E. Ganjeh [c,*]

[a] Materials Division, Mechanical Engineering Department, K.N. Toosi University of Technology, Tehran, Iran
[b] Department of Electrical and Electronics Engineering, UNAM-National Institute of Materials Science and Nanotechnology, Bilkent University, Ankara 06800, Turkey
[c] Materials Division, Faculty of Mechanical Engineering, K.N. Toosi University of Technology, Tehran, Iran

ARTICLE INFO

Article history:
Received 2 August 2013
Accepted 26 October 2013
Available online 1 November 2013

Keywords:
Powder metallurgy
Microstructure
Transverse rapture strength
Fracture

ABSTRACT

Application of powder metallurgy technique, a method presenting both economic and technical concepts for producing sintered parts, has been expanding in automobile and other engineering industries. Powder metallurgy parts usually possess residual porosity in their microstructures deteriorating mechanical performance. There have been many solutions to increasing of strength in these parts such as applying different heat treatment or adding alloying elements. It is well known that Fe–Cu–C is the one of main alloying system for both increasing the strength and decreasing cost of them. In this study, the microstructure, mechanical properties (transverse rapture strength and hardness), crack behavior and fracture modes of a low alloy Fe–Cr powder (Astaloy CrA) with different amount of copper (0, 1 and 2 wt.%) and carbon, in form of graphite (0.45, 0.6 and 0.8 wt.%) sintered at conventional condition have been investigated. Microstructural evolution showed adding copper and graphite as alloying elements could generate widespread of strength (857–1380 MPa) and hardness (170–295 HV5). Developing different phases in microstructure was the main reason for various mechanical properties. Crack coalescence phenomenon leads to fracturing with ductile (at sinter-necks) and brittle morphology. Micro-mechanism of fracture related to transparticle and interparticle crack propagation.

1. Introduction

Powder metallurgy (PM) offers a versatile and efficient method for producing engineering parts and components, especially for application in heavy-duty components like gears, piston and connecting rods; today the fraction is rather between 70% and 80%. PM technique has been developed rapidly in recent years as a profitable technology owing to attractive features such as good strength, easy formability, near net-shape manufacturability and competitive cost [1]. One of the main advantages of the PM technology is simplicity of mixing different metal powders and composing new materials with unique physical and mechanical properties that could not be achieved by conventional melting-casting processes. Sintered low-alloyed PM steels are utilized in many industries such as automotive parts, honeycombs structure, power tools, computers, medical instruments and defense. It has continued to displace the competing cast or wrought technologies in automotive applications [2,3].

Diffusing the alloying additive materials occur through sintering process and contact regions between particles form metallurgical bonds known as sinter necks. Consequently, PM parts usually consisted of the sinter necks and residual porosity [4,5] as an inherent property. Often, sinter necks and pores are the weakest areas in cross section and possibly the eventual location for crack initiation, propagation and fracturing. Nature of the pores and sinter necks are controlled by several processing variables such as porosity level and morphology, alloying additions, homogeneous or heterogeneous microstructures and sintering processes. The fraction, size, distribution and morphology of the pores have a profound impact on mechanical behavior. In general, the porosity in sintered parts is bimodal and can be classified as primary (open pores) or secondary (closed pores). Primary ones consist of larger pores, interconnected, which result in less densification during sintering. Secondary pores contain much smaller ones caused by liquid phase sintering (LPS) of one or more alloying additions forming during sintering. It promotes the homogeneous distribution of the alloying elements through sintering process. An example of an alloying element generating the LPS condition is copper. Upon melting, its particles leave behind small, rounded "secondary" pores with a size approximating of original copper particles [6].

It is well known that the Fe–Cu–C is the one of main alloying system for both increasing the strength and lowering the cost of PM parts [7]. Combination of oxidation sensitive elements to reduce their chemical activity can be basically made in two ways:

* Corresponding author. Address: No. 15-19, Pardis Street, Mollasadra Avenue, Vanak Square, P.O. Box 19395-1999, Tehran, Iran. Tel.: +98 2188674741.
E-mail address: navidganjehie@sina.kntu.ac.ir (E. Ganjeh).

0261-3069/$ - see front matter © 2013 Elsevier Ltd. All rights reserved.
http://dx.doi.org/10.1016/j.matdes.2013.10.072

with fully pre-alloyed iron powders such as the common Cr pre-alloyed grades (e.g. Astaloy CrA), or by using liquid phase sintering (LPS) agent. Astaloy CrA, one of the commercially available low alloy steel powders, can be sintered and subsequently heat treated in many atmospheres. It is a partially pre-alloyed powder for metal powder component production suitable for medium to high performance. By selecting different additions of copper as well as the carbon content the properties can be tailored for enhancing the mechanical performance. Compressive strength can be increased after sintering with additions of graphite. Copper forms a liquid phase during sintering and increases the strength [8].

Matrix microstructure also plays an important role in the deformation and fracture behavior of PM alloys. In particular, the alloying elements and the heat treatments may produce different effects, such as embrittlement of microstructure, formation of a heterogeneous microstructure or rounding of pores because of the liquid phase formation during sintering. All these aspects clearly influence the deformation and fracture behavior of PM alloys since microstructure determines the material's response to the local stress state induced by the pores [5,9–12].

The alloying method (pre-mixed, pre-alloyed and diffusion bonded [10,11,13]) used to manufacturing the PM parts has a significant effect on response of it under different loads due to local chemical composition and resulting local hardenability areas such as the sinter necks [14]. Today, demands for production of parts subjected to high mechanical loads and complex forces, e.g. engine parts and transmission gears need for the availability of dynamic or static properties such as fatigue and bending behavior, respectively [15,16]. The three-point bending (TPB) test is a widespread method for measuring the strength of PM parts possessing low ductility. It is more convenient and faster than the fatigue test for evaluating the crack behavior and fracture modes. The tensile test is difficult for brittle materials due to breaking of specimens around the gripper entitled as gauge's length. As a result, the bending test is more appropriate for testing brittle materials that stress–strain curves show linear elastic behavior up to failure [17]. Not only, the TPB test is used for evolution bending properties of porous sintered steels but also it is suitable for assessment of bending property, ductility, compressive strength and measuring quantitative crack growth for composites [18], polymers [19] and thin films [20].

Influence of composition and processing conditions on the microstructure and properties of Astaloy CrA has been investigated by Frykholm and Litström [21]. Conventional sintering (low cooling rate) result in the microstructure is primarily consists of pearlite which percentage of this phase fluctuates with increasing carbon and copper. Also, slight fraction of ferrite is reported at low carbon addition. The more carbon and copper contents associate with high cooling rate, the more probable to establishing the martensite/bainite phases will be created.

In a research work which had done by Pavanati and colleagues [22], the influence of plasma (UIP) and furnace (UIF) sintering on AISI 310 stainless steel under the TPB test was evaluated. Plasma sintering involves heating a sample under a controlled atmosphere at the sintering temperature using an abnormal glow discharge as a unique source of energy. Sintering of unalloyed iron in plasma revealed the presence of an abnormal grain microstructure after treatment. UIP samples show a considerably lower bending yield load compared with UIF samples. The tendency for lower yield bending strength for UIP samples can be attributed to the exaggerated grains in their microstructure. Sintering of unalloyed iron in a plasma reactor leads to grain growth. In these samples, two regions should be pointed out: 1. Near the surface, where nucleation of the material fracture probably took place and a state of plane stress is predominant due to weak lateral constraints. Therefore, ductile fracture can easily occur in this region. 2. The core region of the sample, which indicates the mechanism of crack propagation with a state of plane strain, prevails in front of the crack. UIF sample showed dimples with a chisel edge on edges and brittle intergranular fracture is evident in the sample core when subjected to the TPB test.

A scan through the literature reveals that published works have been done on PM samples by the TPB test but a few researchers have investigated the (micro) mechanisms of crack initiation, propagation and fracture. The aim of this research is to study and correlate the relationship between microstructure, fracture surface and mechanical properties under the TPB test in a low alloy Fe–Cr powder (Astaloy CrA) with different amounts of copper (0, 1 and 2 wt.%) and graphite (0.45, 0.6 and 0.8 wt.%) sintered as conventional condition (AS).

2. Materials and experimental procedure

2.1. Raw materials

The base powder employed in this work was a diffusion bonded powder, produced by Höganäs Co. The chemical composition of the powder is shown in Table 1. The raw powder contains of 2 wt.% chromium which it results of dimensional stability and improves compressive strength, mechanical properties and hardness. Role of manganese and sulfur elements in the base powder is an agent (MnS) for developing machining property. This powder has wide application in automobile PM parts such as camshaft pulleys, connecting rods [2] and synchronizer hubs [7].

2.2. Sample preparation

Micro wax (1 wt.%), was added as a lubricant with different copper (0, 1 and 2 wt.%) and graphite (0.45, 0.6 and 0.8 wt.%). The powders were blended in a mixer device during 20 min at a constant speed (18 rpm). Then, mixed powders were compacted in an arbitrary die at room temperature with 600 MPa pressure by single action hydraulic machine (100 tons capacity) and consequently flat un-machined test bars. The outcome of these compactions were production of standard samples with approximate density 7 g/cm^3 duo to most of automotive parts like Peugeot synchronizers gearbox has 6.8–7.1 g/cm^3 density. This criterion has been selected as average pressure for pressing.

2.3. Sintering

Sintering process was done at 1120 °C for 30 min in N_2–10H_2 atmosphere. Finally, these samples were cooled at conventional condition (1/3 °C/s) in controlled atmosphere consist of ammonia (N_2–10H_2). Finally, all of sintered samples have been marked (as-sintered) according to pre-mixed alloying elements.

2.4. Density measurement

The density of all samples was measured according to ASTM: B328. The bulk densities of all specimens were measured in pure water by the Archimedes buoyancy method.

Table 1
Nominal composition of alloying element in iron-base powder (all amount in wt.%).

Fe	C	Cr	Mn	S	Others
Bal.	0.44	2.01	0.54	0.15	>0.11

2.5. Chemical composition analysis

After preparation of sintered samples, optic omission spectrometer (OES-ARL 3460) was done for determining the final chemical composition. The mean value for each sample was measured by averaging a minimum of three points (Table 2).

2.6. Mechanical tests

The TPB and hardness tests were applied for each sample. TPB test was conducted in a tensile machine test Zwick/ Reoll Z050. The specimens with dimensions of $5.7 \times 6.3 \times 31.7\ mm^3$ were machined according to ASTM: B528-12 standard. Hardness measurements were made using a Vickers hardness tester (Wolpert Instron) with a load of 5 kg and a dwell time of 20 s. All mechanical tests were done at room temperature and the test results were typically the average of three experiment. Cross-head speed was set to 1 mm/min and span length (L_p) fixed to 25.5 mm. The schematic of the TPB set up is illustrated in Fig. 1. We used Eq. (1) for measuring the transverse rapture strength (TRS).

$$\sigma = \frac{1.5F.L_p}{bh^2} \quad (1)$$

Which F is the force required to rupture the specimen in (N), L_p is length of specimen span relative to fixture (25.5 mm), b is width of the specimen in (5.7 mm), h is thickness of specimen in (6.3 mm) and σ is the fracture strength in (Mpa).

2.7. Microstructure observations

Samples were mechanically polished and low rates and pressures were selected for grinding and polishing for reduction of eventual effect on porosity morphology. Metallographic observations were carried out using a light optic microscope (LOM) IMI-420 that were made on un-etched and etched micrographs in order to identify and observe the crack growth and microstructure condition. Metallographic samples used for identification of microstructure were etched with 3% Nital. Before fractography observation, samples were ultrasonically cleaned by acetone. The fracture surfaces (transverse cross-sections) were examined by scanning electron microscope (JEOL, Japan) JSM-6360 to characterization the fracture morphologies and moods.

3. Results and discussion

3.1. Microstructure investigation

Fig. 2 shows microstructure of as-sintered samples with various copper (0, 1 and 2 wt.%) and carbon (0.45, 0.6 and 0.8 wt.%) content. There is 11–14% porosity in all of microstructures as an inevitable phenomenon determined with black areas in micrographs.

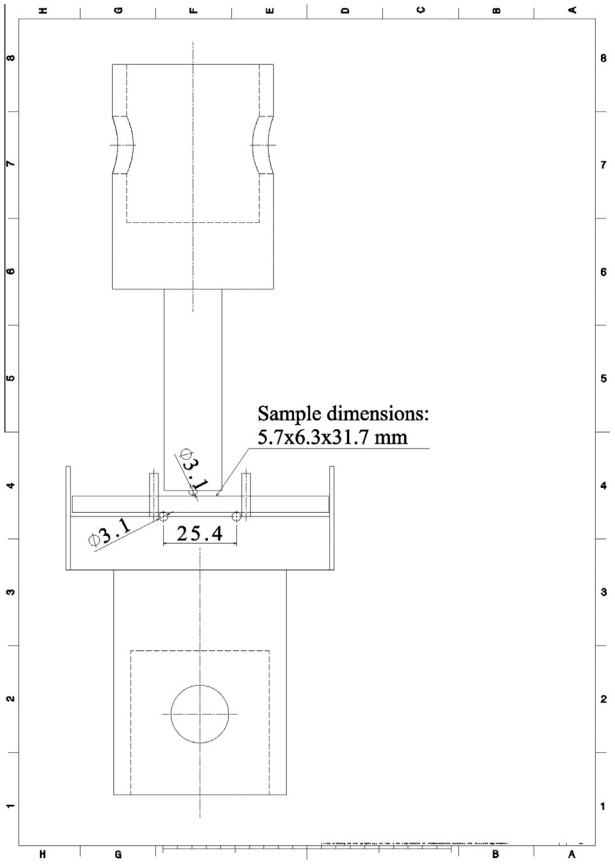

Fig. 1. Schematic of the TPB test.

Primary sample (AS-A1) establishes ferrite – fine pearlite microstructure. Typical micrograph illustrates homogeneous and uniform phase distribution duo to lack of mixing alloying elements. Sintered pre-alloyed powders demonstrate identical microstructure [2,23,24]. Independent of carbon and copper contents, the microstructure mainly consists of pearlite. Some small fraction of ferrite was observed at low amount of carbon. Nucleation and growth of the ferrite will be suppressed if more copper atoms as an austenite stabilizer dissolved in the austenite grains [25]. At subsequent stages, the as-sintered specimens (AS-A6 and AS-A9) are further cooled below the eutectoid temperature and residual austenite regions subsequently transform into pearlite [21]. These parameters do not capability to generate the martensite morphology. The more increasing carbon content, the more pearlite morphology could be developed in the microstructure.

Continuous cooling transformation (CCT) diagrams are beneficial method for describing the behavior of material. Fig. 3 presents

Table 2
Steel base samples marking in accordance to mechanical and chemical properties of sintered parts.

Pre-mixed elements		Sample code	Post-sinter content								Mechanical properties		
Carbon (wt.%)	Copper (wt.%)		Cr	Cu	C	S	Mn	Si	Ni	Mo	F_{TRS} (N)	σ_{TRS} (MPa)	HV(5)
0.45	0	AS-A1	2.01	0.03	0.44	0.15	0.54	0.07	0.04	0.02	5171 ± 20	857.6 ± 4	170.1 ± 10
	1	AS-A2	1.87	1.11	0.46	0.12	0.47	0.07	0.04	0.07	5293 ± 25	877.8 ± 6	184 ± 8
	2	AS-A3	2.18	1.8	0.53	0.11	0.51	0.08	0.04	0.02	6486 ± 35	1075.6 ± 5	228.3 ± 6
0.6	0	AS-A4	1.99	0.02	0.61	0.13	0.54	0.05	0.03	0.02	6204 ± 50	1028.9 ± 7	193 ± 9
	1	AS-A5	1.85	1.05	0.65	0.11	0.41	0.06	0.04	0.04	8353 ± 100	1385.3 ± 16	211 ± 2
	2	AS-A6	2.10	2.01	0.63	0.12	0.49	0.08	0.05	0.02	6943 ± 50	1151.4 ± 6	250.6 ± 5
0.8	0	AS-A7	2.01	0.04	0.87	0.15	0.54	0.07	0.04	0.04	7210 ± 30	1195.7 ± 4	285 ± 9
	1	AS-A8	1.95	1.11	0.79	0.13	0.49	0.07	0.04	0.04	7346 ± 90	1218.3 ± 11	295 ± 10
	2	AS-A9	2.15	1.99	0.83	0.11	0.51	0.06	0.03	0.02	7857 ± 60	1303.0 ± 10	285 ± 7

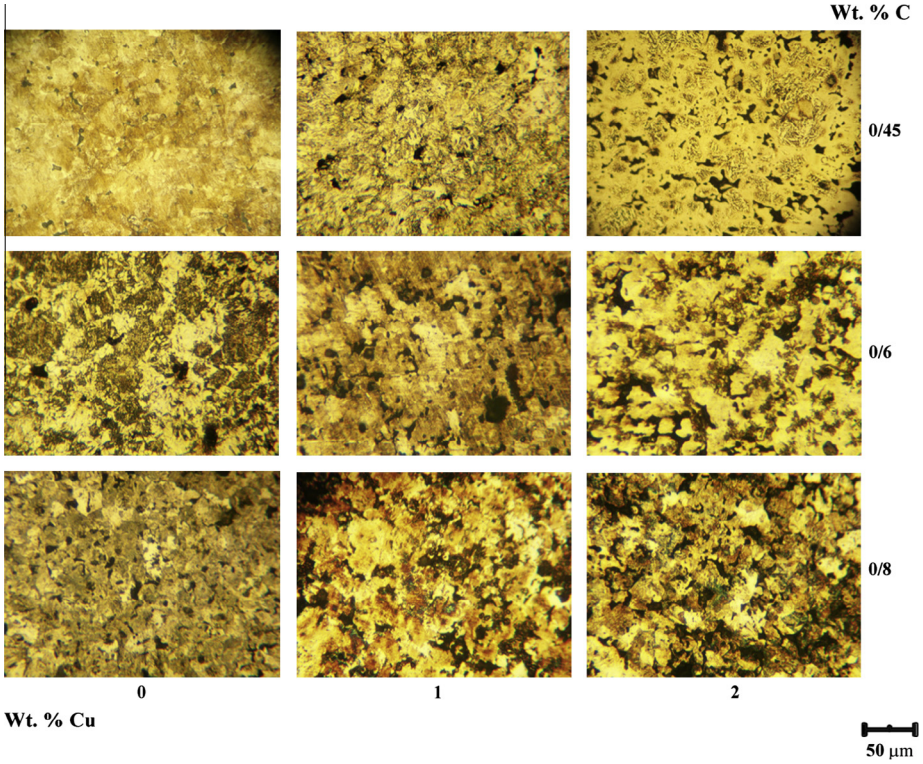

Fig. 2. Optical micrographs of microstructures corresponding to varied copper (0, 1 and 2 wt.%) and carbon (0.45, 0.6 and 0.8 wt.%) content.

the CCT diagrams for Astaloy CrA + 0.5 wt.% C. The major influence of chromium is actually on the eutectoid composition rather than eutectoid temperature. In general, all alloying elements improve hardenability; however, Mo, C and Cr are highly influential [26,27]. Chromium significantly lowers carbon content, and at 1.8 wt.% Cr the eutectoid content is approximately 0.45 wt.% C. Upper this condition, driving forces for cementite formation should increase. It seems that at high C-level, the carbide phases become the leading agents in the growth of a fine pearlitic structure [21]. Therefore, the microstructure of Astaloy CrA with 0.6 and 0.8 wt.% C is mainly fine pearlite with some train of ferrite. Ignoring copper percentage, increasing carbon content has adverse effect on M_s. This microstructure is agreed by many researchers [21,26,27].

Copper additions in accordance with carbon, might shift the C-level when an increase in pearlite is observed. Copper diffused slower than carbon and increases the carbon activity. Thus carbon will redistribute during sintering to level out activity gradients. An increase in the amount of pearlite can therefore be observed for comparably low C-contents, since the actual C-content in the pearlite regions will be higher than the average content. Increasing copper content at a constant carbon percentage, changes the microstructure to a mixture of pearlite, ferrite and diffused copper with small traces of secondary copper particles. Copper as the rudimentary alloying element for direct effect on hardening, formation of PLS and activation of sintering process at below temperatures is proposed. At sintering temperature, it melts and then diffuses into the iron powder particles creating dimensional changes and swelling. It is possible to balance this swelling against the natural shrinkage of the iron powder matrix by adding optimum graphite or nickel and carefully selection of copper content. Also, the copper addition provides a useful solid solution strengthening effect. The more increase in the carbon content, the less amount of copper diffused in the structure. The general trend for the decrease in the solubility of copper with increasing carbon content can be obtained from Fig. 4 [28,29]. Addition of 1 wt.% Cu (AS-A5) establishes mixed pearlite – pre-eutectoid ferrite matrix reinforced by some bainite/martensite phases. This condition is cause of replacing certain pearlite to both bainite and martensite. Further addition of 2 wt.% Cu (AS-A9) has increased martensite content with respect of reducing pearlite islands.

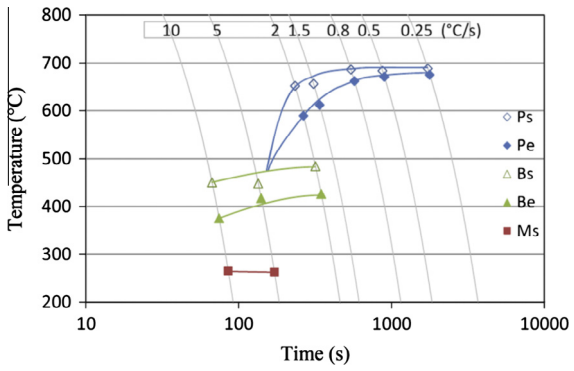

Fig. 3. CCT diagrams for Astaloy CrA-0.5 wt.% C. The diagram shows pearlite start and end (Ps/Pe), bainite start and end (Bs/Be), and martensite start (Ms) [21].

3.2. Mechanical properties

Mechanical properties of samples are listed in Table 2. It is necessary to note that the averages of the results (averages for three test specimens) were reported. Mechanical properties of as-sintered samples are influenced by several factors. Carbon is the most basic and commonly used alloying element to increasing the strength and hardness of the sintered parts. The quantity of graphite mixed in the iron powder varies from 0.2 to 1 wt.% The

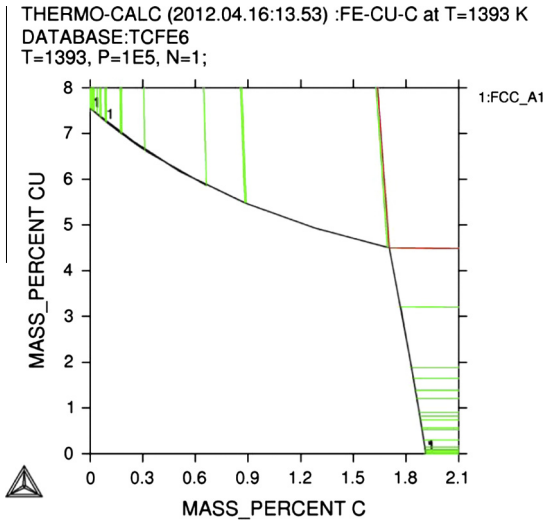

Fig. 4. Solubility of copper with increasing carbon content [29].

structure is mainly pearlitic (Fig. 2) for all carbon levels, but with the presence of some ferrite at 0.45 wt.% C. The increase in strength from 0.6 to 0.8 wt.% carbon is due to reducing of ferrite contents. Further increase in strength is a result of finer pearlite morphology. The transverse rapture strength and hardness have been increased by introducing carbon content in the system. Considering a fixed copper percentage (like 0 wt.%), the former varied 857.6–1195.7 MPa while the latter has 170–285 (HV5) ranges. Development of widespread phases is responsible for different mechanical properties. The microstructure of as-sintered carbon samples have heterogeneous one with different ferrite and pearlite phase contents.

Copper is one of the widely used elements in PM increasing the strength and hardness. Usual amounts of copper admixed are 1.5–3 wt.%. When copper extra-admixed to iron causes swelling, discussed earlier. The transverse rapture strength outcomes demonstrates increasing copper and carbon content to 1 and 0.6 (wt.%) could be beneficial to having bilateral strength (1385.3 MPa) and hardness (211 HV5). Establishing a metallic composite containing of martensite/bainite phases as the reinforcement in a ductile pearlite matrix is the main reason. With further addition of copper, there will be a shift back in strength (17%) due to structure morphology. The foremost reason of declining strength is related to formation of secondary pores duo to adding extremely copper to the system. Consequently, changing carbon and copper content, wide range of mechanical properties could be established. It is an advantage for manufacturing gears duo to diverse hardness values from surface to center part. At the best condition of sintering and alloying elements (AS-A8 sample), the hardness level increased to 285–295 Vickers.

3.3. Fractography analysis

Fractographic analysis is a useful method for studying crack nucleation and propagation during bending test. It is a suitable method for knowing about failure and workability of material. Fracturing actually started by crack initiation and propagation (mode I) until failure the sample (mode II) and is influenced by many factors like, alloying elements, porosity, microstructure and heat treatment. In this section, the former and later discussed comprehensively [30].

3.3.1. Mode I: crack initiation and propagation

Fig. 5 illustrates the porous structure before etching. During the TPB test, the top surface of the sample experiences compression while the opposite surface experiences tension. Micrograph evaluation shows during transition from compression to tension zones, shape of pores become more angular, elongated and sharpened. The material failure in bending is therefore due to the tensile stresses along the surface in tension. According to Fig. 5, it was observed that during sample loading in the TPB test, in the some places near the tension surface cracks could form. Crack initiation and propagation on the surfaces subjected to tensile stress is the major reason for fracture in bending [31].

Several researchers have found that pores and pore clusters act as sites of crack initiation, which can coalesce to form large cracks leading to failure. One may assume that before crack coalescing, the most probable nucleation sites for these microvoids are both pores and relatively large and widely spaced inclusions (e.g.

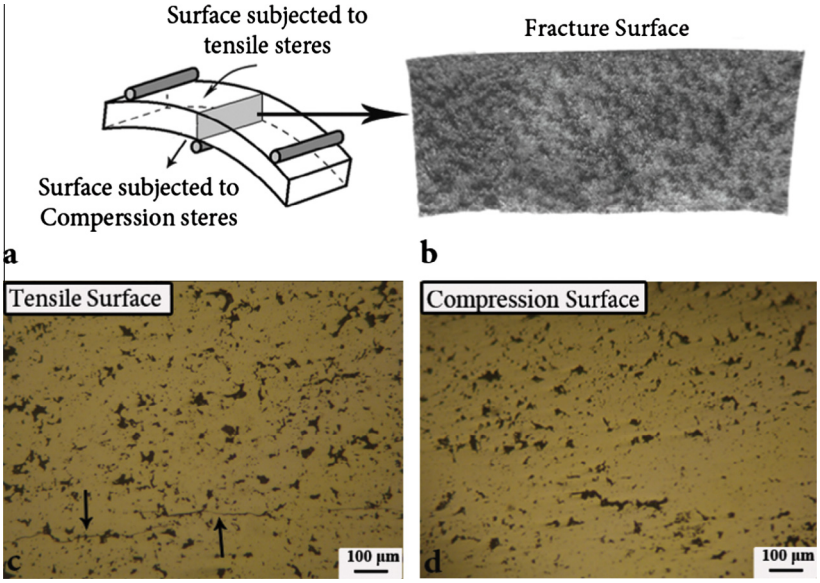

Fig. 5. (a) Schematic of tensile and compression stresses that applied on sample surfaces, (b) macro image of fracture surface, (c) tensile surface with indication of cracks (arrows) and (d) compression surface which do not have any cracks as expect.

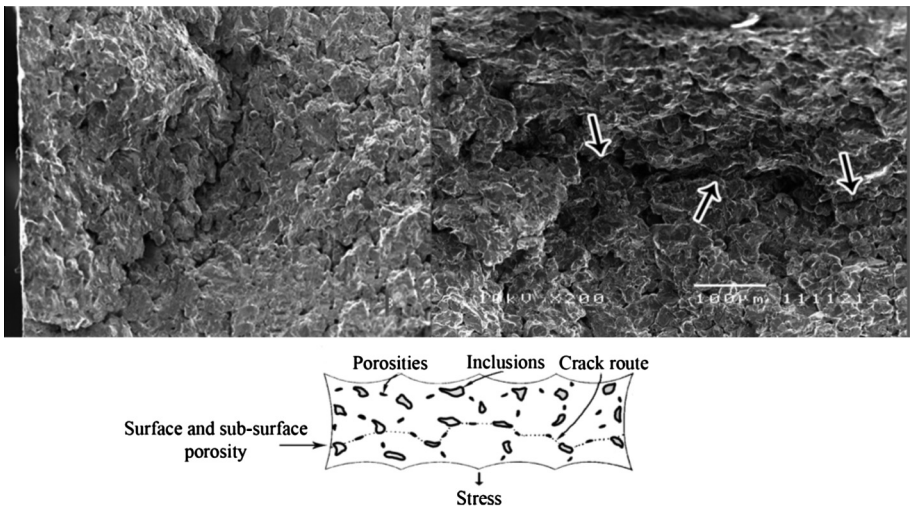

Fig. 6. Crack coalescence, surface and sub surface porosity phenomena that show with arrows.

oxides) [32]. Stress distribution and local strain around pores, cause local deformation, nucleation and crack growth [2,11,33–36]. Surface and sub-surface pores are supplementary reasons for fracture in this test. According to definition [2], in PM parts cracks are nucleate and initiate from surface pores under different static (tensile) and dynamic loading (fatigue). This has been confirmed by several researchers [32,37,38]. Likewise, in this research the examination of fracture surfaces revealed that in many cases initiation sites are constituted by pores located a few microns below the tensile surface, as shown in Fig. 6. Particle fracture, which can occur when bonding between the matrix and inclusion is strong, can accelerate the development of crack growth [32,37]. In addition, elongated pores create condition for crack growth more easily in a tensile surface. With continuing of force, pores will connected from places that have more stress concentration (sharp edges) and after crack coalescence phenomena, fracture occurred in samples.

3.3.2. Mode II: fracture mechanism

According to Fig. 7, both ductile and cleavage features (mixed modes) were observed in the fracture surface of samples. Evaluations of the SEM micrographs show addition of copper and carbon simultaneously, the brittle fracture morphology has occupied the surface due to hard phases generated during sintering. The most important assumption is pearlite morphology as principal phase which has twofold fracture behavior changing with adding different alloying content. It is recognizable that the dominant fracture mode in as-sintered PM samples is cleavage, due to pore existence. In sintered necks, we have ductile fracture at a microscopic scale. This is the main reason for small elongation in PM materials. The mixed fracture modes in the TPB test have also been reported by many researchers [3,38].

Most of the mechanisms discussed the various fracture modes are based on concepts of dislocation interactions and movement, involving crystallographic relationships, slip behavior and plastic

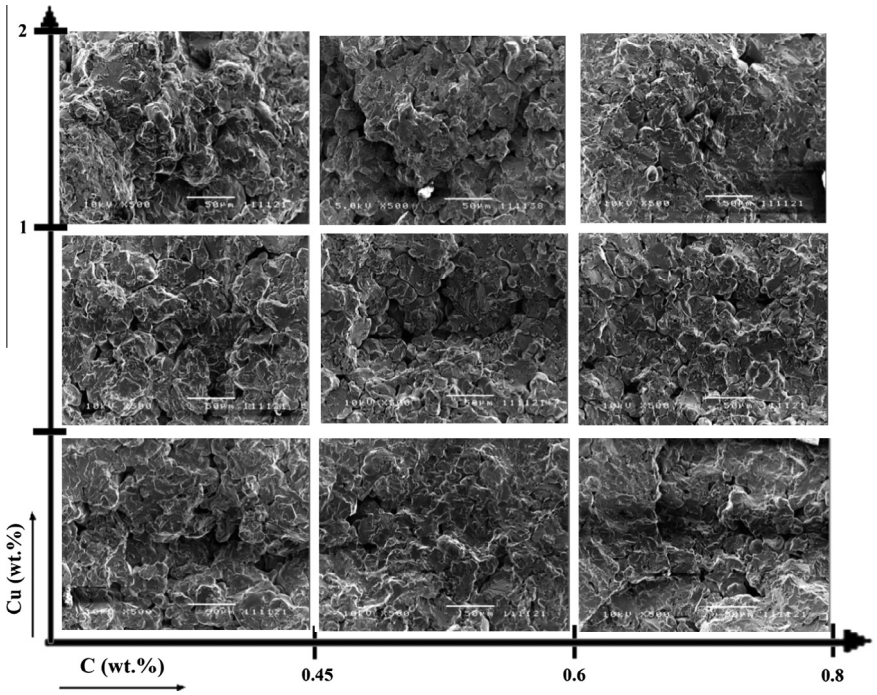

Fig. 7. SEM images from fractured surface for different sintered samples.

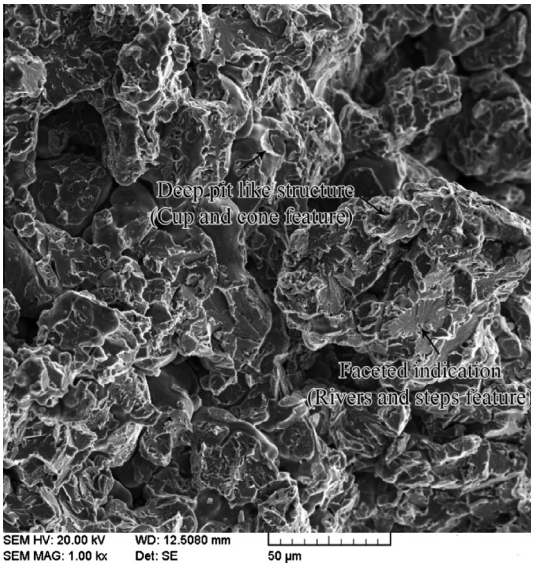

Fig. 8. A typical SEM image of TPB fractured surface for intermediate alloying content showing two feature characteristic.

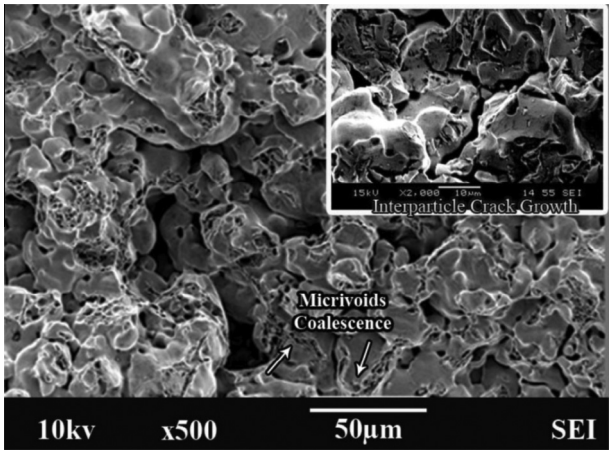

Fig. 9. Fractured of surface with microvoids coalescence fracture mechanism by voids clustering (inset picture is interparticle crack).

deformation [31]. Also, it is important to note that fractured surfaces do not have very modifications at macro scale but at higher magnification the fracture mechanism could be examined more precise. In this section, fracture mechanisms are discussed at microscopic scale depending on fractographic concept.

Sintered materials may be considered structures composed of necks and particles. If micro mechanisms of failure occur at the particle necks, the fracture mode is ductile due to neck formation depending on the processing parameters. However, if sintered materials have wide particle necks and also an appropriate pore size and morphology, fracture can run through the particles. For sintered materials, particle cleavage frequently means favorable behavior because it indicates strong sintering contacts [13].

Several models have been proposed [13,32,37] to describe cleavage fracture. It is summarized in the following stages: under an external load, micro cracks are nucleated ahead of a dislocation pile-up and they grow through the grain of the respective particle. Then those cracks pass through the first grain boundary they encounter. When these barriers are overcome, fracture continues through similar obstacles as far as the external load is applied. When the crack has crossed the first grain and reaches the boundaries, rivers appear as cracks crossing the grain through

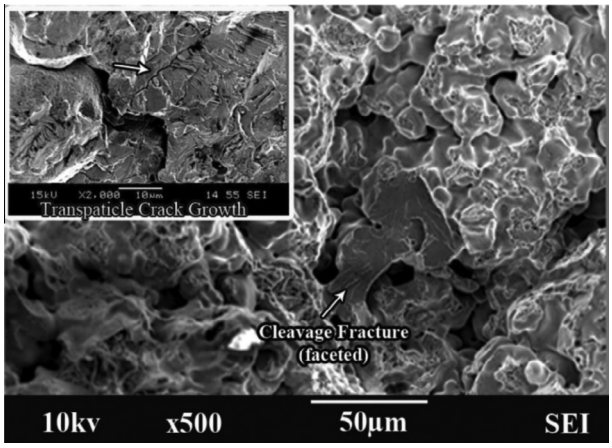

Fig. 10. Fractured surface (local martensite/bainite in pearlite matrix) with basically transgranular cleavage (inset picture is transparticle crack).

parallel planes that constitute river and step features. These appearance fractures featured in these zones are dominantly faceted according to Fig. 8. Also, the presence of a deep pit like structure is an indication of the formation of ridges during the cup and cone fracture in ductile fracture (Fig. 8). It is not logical to relate one feature to unique microstructure.

When powder particles connected together in some places, the mode of fracture changed to ductile at sinter necks. In Fig. 9 it is seen that ductile fracture occurred by micro void coalescence should be the result of forming limited diffusion of powders duo to their attributes. These voids are suitable place for crack coalescence by raising local stresses. At this condition, cracks walking occurred through interparticle (known as intergranular fracture, inset Fig. 9). In addition, there are possibility which some cracks routes followed among powders (known as transgranular fracture, inset Fig. 10). When the fracture mode is transgranular, the combination of loads (tensile and compression) and microstructure representatives (e.g. martensite/bainite), which are synchronized applied to small part of specimens and interference in fracture mechanism are main abjections [32]. It had studied by Straffelini and Fontanari [12] which in the PM steels, pores act as internal defects for dimpled fracture, and the nominal plastic strain needed for the initiation of voids at the interparticle necks is very low.

4. Conclusions

In this research, low alloy steel powder (Astaloy CrA) with different amount of copper (0, 1 and 2 wt.%) and carbon (0.45, 0.6 and 0.8 wt.%) were subjected to microstructural analysis and mechanical tests (TPB and hardness), in order to investigate the microstructure correlation, crack growth behavior, modes of fracture and bending properties. The following conclusions can be drawn:

1. The dominant morphology of all as-sintered samples consisted of pearlite changing with the copper and carbon content. The primary perlite + ferrite become transformed to martensite/bainite by the increasing copper content.
2. Mechanical properties of the base as-sintered samples were measured 857 MPa and 170 HV5 for TRS and hardness, respectively. TRS improved as 38% (1385 MPa) by adding 0.6 carbon and 1 copper (AS-A5, wt.%). On the other hand, the maximum hardness level was obtained for AS-A8 (0.8 wt.% C + 1 wt.% Cu) enhanced 41%. The ideal mechanical performance for as-sintered automotive parts related to AS-A5 sample.

3. According to microscopic observations, due to different applied stresses, some elongated porosity and cracks were detected on the cross section of the specimens. In part of the sample that was under compression, the pores were compacted, but in the part under tension, the cracks occurred. Pores located at the surface or just below it are prone to nucleation and crack growth.
4. Fractured surfaces of the TPB test contain both ductile and cleavage morphology. Generally, pore existence in the PM materials activates cleavage feature more than ductile. Therefore, fractography analyses showed that the dominant fracture mechanism is cleavage.
5. Fracture mechanisms are dependent on different phases formed during sintering. Different structures result in different proportions of fracture types. By increasing the strength, the dominant fracture micro-mechanism changed from intergranular (with voids growth mechanism) to transparticle.

Acknowledgements

The authors would like to thank the faculty of aerospace engineering for designing and manufacturing the fixtures, materials research center and chemical laboratory of SAPCo and Lut PM Factory for cooperation, manufacturing and providing the experimental facilities. The authors would like to thank Dr. A. Zolriasatein for their kind scientific editions on the preparation of this manuscript.

References

[1] Kandavel TK, Chandramouli R, Karthikeyan P. Influence of alloying elements and density on aqueous corrosion behaviour of some sintered low alloy steels. Mater Des 2012;40:336–42.
[2] German RM. Powder metallurgy of iron and steel. USA: John Wily & Sons; 1998.
[3] Rosso M, Dobrzański LA, Otrêba J, Grande MA. Mechanical properties and microstructural characteristic of sinter-hardened steels. Arch Mater Sci Eng 2009;35:117–24.
[4] Deng X, Piotrowski G, Chawla N, Narasimhan KS. Fatigue crack growth behavior of hybrid and prealloyed sintered steels Part II. Fatigue behavior. Mater Sci Eng A 2008;491:28–38.
[5] Ganjeh E, Khorsand H, Ghaffari M. Quality study of crack growth in iron-based powder metallurgy samples by three-point bending test. In: Advanced in applied physics and material science congress. Antalya, Turkey; 2011.
[6] Chawla N, Williams JJ, Deng X, McClimon C, Hunter L, Lau SH. Three-dimensional characterization and modeling of porosity in Pm steels. Int J Powder Metall 2009;45:19–26.
[7] Larsson C, Engström U. High performance sinter-hardening materials for synchronising hubs. Powder Metall 2012;55:88–91.
[8] Bekoz N, Oktay E. Effect of heat treatment on mechanical properties of low alloy steel foams. Mater Des 2013;51:212–8.
[9] Straffelini G, Fontanari V, Molinari A. Impact fracture toughness of porous alloys between room temperature and −60 °C. Mater Sci Eng A 1999;272:389–97.
[10] Abdoos H, Khorsand H, Shahani AR. Fatigue behavior of diffusion bonded powder metallurgy steel with heterogeneous microstructure. Mater Des 2009;30:1026–31.
[11] Slesar M, Dudrova E, Rudnayova E. Plain porosity as a microstructural characteristic of sintered materials. Powder Metall Int 1992;24:232–7.
[12] Straffelini G, Fontanari V. Stress state dependent fracture behaviour of porous PM steels. Eng Fract Mech 2011;78:1067–76.
[13] Campos M, Torralba JM. Fracture micromechanism in low alloyed chromium-molybdenum sintered steels depending on static or dynamic applied loads. In: International conference DF PM. Stará Lesná, Slovak Republic; 2002.
[14] Murphy TF. Evaluation of PM fracture surfaces using quantitative fractography. Int J Powder Metall 2009;45:49–61.
[15] Khorsand H, Habibi SM, Yoozbashizade H, Janghorban K, Reihani SMS, Seraji HR, et al. The role of heat treatment on wear behavior of powder metallurgy low alloy steels. Mater Des 2002;23:667–70.
[16] Khorsand H, Habibi SM, Janghorban K, Yoozbashizade H, Reihani SMS. Fatigue of sintered steels (Fe–1.5 Mo–3 Mn–0.7 C). Mater Struct 2004;37:335–41.
[17] Udomphol T. Laboratory 7: Bend testing: Mechanical Metallurgy Laboratory; 2007.
[18] Carbajal N, Mujika F. Determination of compressive strength of unidirectional composites by three-point bending tests. Polym Test 2009;28:150–6.
[19] Loya JA, Villa EI, Saez JF. Crack-front propagation during three-point-bending tests of polymethyl-methacrylate beams. Polym Test 2010;29:113–8.
[20] Jiangu Z, Lu FX, Tang WZ, Wang SG, Tong YM, Huang TB, et al. Accurate measurement of fracture toughness of free standing diamond films by three-point bending tests with sharp pre-cracked specimens. Diam Relat Mater 2000;9:1734–8.
[21] Frykholm R, Litström O. Influence of composition and processing conditions on the microstructure and properties of Astaloy CrA. World PM. Yokohama, Japan; October 18, 2012.
[22] Pavanati HC, Straffelini G, Maliska AM, Klein AN. Microstructural and mechanical characterization of iron samples sintered in DC plasma. Mater Sci Eng A 2008;474:15–23.
[23] Salak A. Ferrous powder metallurgy. Cambridge: Cambridge International Science Publishing; 1997.
[24] Lenel FV. Powder metallurgy: principles and applications. Metal Powder Industry Publication; 1980.
[25] Wang WF. Effect of alloying elements and processing factors on the microstructure and hardness of sintered and induction-hardened Fe–C–Cu alloys. Mater Sci Eng A 2005;402:92–7.
[26] Hatami S, Malakizadi A, Nyborg L, Wallin D. Critical aspects of sinter-hardening of prealloyed Cr–Mo steel. J Mater Process Technol 2010;210:1180–9.
[27] Teimouri M, Ahmadi M, Pirayesh N, Aliofkhazraei M, Khoee MM, Khorsand H, et al. Study of corrosion behavior for nitrocarburized sintered astaloy CrM® +C. J Alloy Compd 2009;477:591–5.
[28] Jamil SJ, Chadwick GA. Investigation and analysis of liquid phase sintering of Fe–Cu and Fe–Cu–C compacts. Powder Metall 1985;28:65–71.
[29] Jonnalagadda KP. Influence of graphite type on copper diffusion in P/M copper steels. Stockholm: KTH; 2012.
[30] Ganjeh E, Sarkhosh H. Microstructural, mechanical and fractographical study of titanium-CP and Ti–6Al–4V similar brazing with Ti-based filler. Mater Sci Eng A 2013;559:119–29.
[31] Dieter GE. Mechnical metallurgy. 3rd ed. USA: Mc Graw Hill; 2001.
[32] Drar H, Bergmark A. Load rate influence on the fracture morphology of ductile steel. Eng Fract Mech 1993;46:225–33.
[33] Danninger H, Jangg G, Weiss B, Stickler R. Microstructure and mechanical properties of sintered iron part i: basic considerations and review of literature. Powder Metall Int 1993;25:111–7.
[34] Danninger H, Spoljaric D, Weiss B. Microstructural features limiting the performance of P/M steels. Int J Powder Metall 1997;33:43–53.
[35] Williams JJ, Deng X, Chawla N. Effect of residual surface stress on the fatigue behavior of a low-alloy powder metallurgy steel. Int J Fatigue 2007;29:1978–84.
[36] Deng X, Piotrowski G, Chawla N, Narasimhan KS. Fatigue crack growth behavior of hybrid and prealloyed sintered steels Part I. Microstructure characterization. Mater Sci Eng A 2008;491:19–27.
[37] Drar H. Metallographic and fractographic examination of fatigue loaded PM-steel with and without MnS additive. Mater Charact 2000;45:211–20.
[38] Trabadelo V, Gimenez S, Iturriza I. Development of powder metallurgy T42 high speed steel for structural applications. J Mater Process Technol 2008;202:521–7.